ACS Catalysis

Research Article

pubs.acs.org/acscatalysis

Coverage-Dependent CO Adsorption and Dissociation Mechanisms on Iron Surfaces from DFT Computations

Tao Wang,[†] Xin-Xin Tian,[‡] Yong-Wang Li,[‡] Jianguo Wang,[‡] Matthias Beller,[†] and Haijun Jiao*[,†,‡]

[†]Leibniz-Institut für Katalyse e.V. an der Universität Rostock, Albert-Einstein Strasse 29a, 18059 Rostock, Germany

[‡]State Key Laboratory of Coal Conversion, Institute of Coal Chemistry, Chinese Academy of Sciences, Taiyuan, Shanxi 030001, People's Republic of China

Supporting Information

ABSTRACT: CO adsorption structures and energetics on the iron (100), (110), (111), (210), (211), and (310) surfaces from the lowest coverage up to saturation have been computed using spin-polarized density functional theory and ab initio thermodynamics. It is found that different adsorption configurations on each of these surfaces at high coverage can coexist. The stepwise adsorption energies and dissociation barriers at different coverage reveal equilibriums between desorption and dissociation of adsorbed CO molecules. Only molecular CO adsorption is possible at very high coverage and only dissociative CO adsorption at very low coverage, whereas mixed molecular and dissociative CO adsorption becomes possible at medium coverage. The computed stable adsorption configurations and the respective C−O and Fe−C stretching frequencies as well as desorption temperatures on the (100), (110), and (111) surfaces agree very well with the available experimental data. Such agreements between theory and experiment validate our computational methods and allow us to reasonably predict the experimentally unknown CO activation mechanisms on the (210), (211), and (310) surfaces. Our results might provide some references for the study of CO related reaction mechanisms.

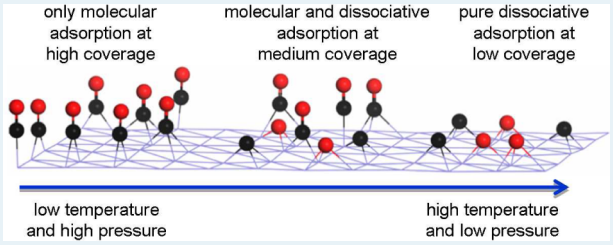

KEYWORDS: *DFT, CO, adsorption, dissociation, iron surfaces, high coverage*

1. INTRODUCTION

As a very important and useful basic chemical, carbon monoxide (CO) has found wide applications in energy societies as well as value-added bulk and fine chemical productions. The most representative examples are Fischer−Tropsch synthesis (FTS),[1] alcohol synthesis, and hydrogen production from the water−gas shift (WGS) reaction.[2] To understand these key processes deeply, it is very necessary and essential to study CO adsorption and dissociation mechanisms on the surfaces of heterogeneous catalysts. Because of the significant relevance of CH_x formation in the FTS process,[3,4] CO adsorption and dissociation mechanisms on iron surfaces have attracted great attention from academic researchers and for industrial applications. More specifically, the adsorption, desorption, and dissociation of CO on iron surfaces are very essential steps in association with the catalytic activities. In the last two decades, diverse experimental techniques and state of the art theoretical calculations have been explored to investigate the interaction of CO with iron single crystalline surfaces.

On the Fe(110) surface, Yoshida and Somorjai[5] found an ordered molecular CO adsorption at 270 K and a dissociative adsorption at 400 K by using low-energy electron diffraction (LEED) and thermal desorption spectroscopy (TDS). Broden et al.[6] also found a molecular CO adsorption on the Fe(110) surface at room temperature and a dissociative adsorption at 385 K in an ultraviolet photoemission spectroscopy and LEED study. Erley[7] investigated CO chemisorption on the Fe(110) surface at 120 K by using LEED and high resolution electron energy loss spectroscopy (HREELS) and found the shifts of the Fe−C stretching frequency from 456 to 500 cm^{-1} up to 0.7 L (0.25 ML) and from 484 to 444 cm^{-1} at 0.7−1.5 L (0.5 ML) as well as the C−O stretching frequency from 1890 to 1985 cm^{-1} with an increase in exposure. Gonzalez et al.[8] studied CO adsorption and desorption kinetics on the Fe(110) surface by using TDS and found a molecular CO desorption at 400−420 K and a recombinative desorption at 675−800 K, and that surface defects facilitate CO dissociation. In a laser-induced thermal desorption study of CO on the Fe(110) surface, Wedler et al.[9] found that the desorption maximum amplitude depends on laser pulse intensity and CO coverage. A work function study (WF)[10] revealed a facile equilibrium between adsorption and desorption at room temperature and dissociation above 380 K for CO on the Fe(110) surface.

On the Fe(100) surface, three molecular CO adsorption states (α_1, α_2, and α_3) at about 220−250, 306−340, and 400−440 K as well as one recombinative desorption of dissociated C and O atoms at around 750−820 K (β state) were detected by applying surface science techniques such as X-ray photoelectron spectroscopy (XPS) and temperature-programmed desorption (TPD),[11−13] and CO dissociation was observed at about 440 K.

Received: March 4, 2014
Revised: April 29, 2014
Published: May 7, 2014

   dx.doi.org/10.1021/cs500287r | ACS Catal. 2014, 4, 1991−2005

Further study by applying XPS, TPD, X-ray photoelectron diffraction,[14] near-edge X-ray absorption fine structure spectroscopy,[15−17] and HREELS[18,19] identified the 4-fold hollow site with an unusually low CO stretching frequency of 1210 cm^{-1} as the most stable adsorption configuration (α_3), representing the CO dissociation precursor state. By using HREELS and temperature-programmed surface reaction techniques, Lu et al.[20] studied CO adsorption and dissociation on the Fe(100) surface at 423 K and found CO dissociation at coverage lower than 0.15 monolayer (ML) and CO desorption at coverage higher than 0.15 ML. The bonding mechanism of the predissociative hollow (α_3) phase and the nondissociative atop (α_1) phase of CO on the Fe(100) surface was studied by Gladh et al.[21] by using X-ray emission spectroscopy and density functional theory (DFT) calculations, and a π-donation/π^* back-donation scheme is proposed for CO in the 4-fold hollow site. Wilcox et al.[22] systematically studied the adsorption mechanism and electronic structure of CO on the FeCo(100) alloys and compared it with those on the pure Fe(001) and Co(0001) surfaces.

In a combined HREELS, LEED, TDS and WF study of CO on the Fe(111) surface, Seip et al.[23] found the sharp peak at 400 K (α_2 state) in TDS belonging to CO adsorption at the shallow hollow site, the α_1 state at high exposure belonging to CO adsorption at the atop and deep-hollow sites, and the β state coming from the recombinative desorption of the adsorbed C and O atoms. A similar study of CO adsorption on the Fe(111) surface by applying low-temperature exposure and high-resolution data by Bartosch et al.[24] confirmed three CO adsorption states and found a previously unobserved CO stretching vibration at 1325 cm^{-1}. In a TPD and time-resolved electron energy loss spectroscopy study of CO adsorption on the Fe(111) surface, Whitman et al.[25] found that CO site occupancy depends on coverage and temperature.

In addition to the extensive experimental studies, CO adsorption on iron single crystalline surfaces also has been widely studied theoretically. Early studies in the 1980s applied mainly semiempirical[26,27] and Hatree−Fock[28] methods. By using infinite slab and finite cluster models to study CO adsorption on the Fe(001) surface, Nayak et al.[29] found that the 4-fold hollow site is the energetically most preferred adsorption site, followed by the atop and bridge sites. Sorescu et al.[30] computed the adsorption of CO, C, and O atoms as well as CO dissociation on the Fe(100) surface and found that CO on the 4-fold site (α_3 state in TPD) is the most stable and has a dissociation barrier in the range of 1.06−1.22 eV, whereas CO on the bridge site (α_2 state) is more stable than on the atop site (α_1 state) at low coverage, and the atop site becomes more stable than the bridge site at high coverage. Bromfield et al.[31] studied CO interaction on the Fe(100) surface and found that CO adsorption and dissociation are coverage dependent. On the Fe(100) surface, Elahifard et al.[32] proposed CO direct dissociation at low coverage and H-assisted CO dissociation at high coverage.

The DFT study of CO adsorption on the Fe(110) surface at different coverage by Stibor et al.[33] revealed that CO adsorption on the top site is the most stable at low coverage but on the long bridge site becomes the most stable at high coverage. Because of the disagreement with the favored top adsorption configurations at high coverage on the basis of the detected CO vibrational frequencies, they attributed this disagreement to the overestimation of the stability of the long bridge adsorption configuration by the DFT method. By applying a different exchange and correlation functional, Jiang and Carter[34] studied CO adsorption and dissociation on the Fe(110) surface, and their results show that the PW91, PBE, RPBE, and PKZB methods can yield the correct site preference at 0.25 ML, but only PKZB predicts the correct site preference at 0.5 ML. They also reported a CO dissociation barrier of 1.52 eV on the top site on the Fe(110) surface at 0.25 ML with PBE. Sun et al.[35] investigated the spin-resolved electronic states of CO on the Fe(110) surface using spin-polarized metastable-atom de-excitation spectroscopy (SPMDS) and first-principles DFT and found the existence of the adsorbate-induced $2\pi^*$ state in addition to CO 4σ and 5σ /1π states.

On the Fe(111) surface, Chen et al.[36] carried out a systematic DFT study of CO adsorption at different coverage and revealed that shallow hollow adsorption is most stable at 1/3 and 1/2 ML; shallow hollow and bridge adsorptions coexist at 1 ML, and bent atop and triply capping adsorptions are most favorable at 2 ML. Huo et al.[37] studied CO dissociation on the clean and hydrogen-precovered Fe(111) surfaces by DFT calculations and revealed H-assisted CO dissociation to be more favorable than CO direct dissociation. A similar result about H-assisted CO dissociation on Fe(111) was also reported by Li et al.[38]

CO chemisorption on the Fe(211) surface was reported by Borthwick et al.[39] using first-principles DFT and a single-crystal adsorption calorimetric method. In their study, the adsorption state at the 3-fold site involving one top-layer and two second-layer metal atoms is most stable. They also found that CO dissociation is particularly facile, and the Fe(211) surface is optimal for FTS. Lo et al.[40] studied CO adsorption and dissociation on the stepped Fe(310) surface by using the DFT method at 0.25 and 0.50 ML and found significant contributions of coverage to the overall CO decomposition rate at 0.5 ML. Sorescu[41] studied CO adsorption, diffusion, and activation on the kinked Fe(710) and Fe(310) surfaces and found the smallest activation barriers for CO dissociation in the regime of low coverage compared with the Fe(100), Fe(110), Fe(111), and Fe(211) surfaces.

Despite these extensive DFT studies about CO adsorption on iron single crystalline surfaces, it is still difficult for a systematic comparison among different surfaces because those data have been obtained by using very diverse models and methods. Furthermore, the coverage-dependent CO adsorption and dissociation, apart from our recent work,[42] has not been considered previously. Because the surfaces of FTS catalysts have been proved to be CO-precovered experimentally,[43−45] studies of high-coverage CO activation are essential to understand the initial steps of the FTS process as well as reactions involving CO deeply. Because the active phases of catalysts in heterogeneous catalysis are polycrystalline and always very complex, the reasonable way to get a deep and reasonable understanding into the active sites and catalytic properties is to consider all possibilities. We therefore performed a systematic study of CO adsorption, dissociation, and desorption on iron (110), (111), (210), (211), and (310) surfaces at different coverages using the same DFT methodology. For a general comparison, we included our results of CO adsorption and dissociation on the (100) surface. Our goal is to reveal the coverage-dependent adsorption, dissociation, and desorption processes and, finally, to present the initial state of CO activation on iron surfaces, which will provide some references for the studies of CO related reaction mechanisms.

dx.doi.org/10.1021/cs500287r | ACS Catal. 2014, 4, 1991−2005

2. COMPUTATIONAL METHODS AND MODELS

2.1. Methods. All calculations were performed by applying the plane-wave-based DFT method implemented in the Vienna ab initio simulation package (VASP).[46,47] Periodic slab models were used to model the catalyst surfaces. The electron ion interaction was described with the projector augmented wave (PAW) method.[48,49] The electron exchange and correlation energy was treated within the generalized gradient approximation in the Perdew−Burke−Ernzerhof formalism (GGA-PBE).[50] Spin-polarization was included for iron systems to correctly account for the magnetic properties, and this was found essential for an accurate description of adsorption energies.[51] To acquire accurate energies with errors of <1 meV per atom, an energy cutoff of 400 eV and a second-order Methfessel−Paxton[52] electron smearing with σ = 0.2 eV were used. A vacuum layer of 10 Å was set between the periodically repeated slabs to avoid strong interactions.

The adsorption energy (E_{ads}) of one CO molecule is defined as $E_{ads} = E_{CO/slab} - [E_{slab} + E_{CO}]$, where $E_{CO/slab}$ is the total energy of the slab with one CO adsorption, E_{slab} is the total energy of the bare slab, and E_{CO} is the total energy of a free CO molecule in the gas phase; and a more negative E_{ads} indicates a stronger adsorption. To consider the coverage-dependent CO adsorption and dissociation, CO was added to the surfaces one-by-one on the basis of the most stable adsorption structure of one CO, that is, one additional CO molecule was added to the previous most stable one for getting the next most stable one after considering different adsorption sites. For getting the saturation coverage, stepwise adsorption energy (ΔE_{ads}) was applied, that is, $\Delta E_{ads} = E_{(CO)n+1/slab} - [E_{(CO)n/slab} + E_{CO}]$, where a positive ΔE_{ads} for n + 1 adsorbed CO molecules indicates the saturated adsorption with nCO molecules. Our stepwise adsorption energy defines the change in the adsorption energy by adding one more species to the surface, whereas the differential energy of adsorption defines the change in the average adsorption energy per coverage as a function of the coverage.[53]

To locate the CO dissociation transition states on iron surfaces, the nudged elastic band method[54] was applied, and the CO stretching frequencies were analyzed to characterize a transition state with only one imaginary frequency. The CO dissociation barrier (E_a) is defined as $E_a = E_{TS} - E_{IS}$, and the reaction energy (E_r) is defined as $E_r = E_{FS} - E_{IS}$, where E_{IS}, E_{FS}, and E_{TS} represent the total energy of the initial adsorbed CO molecule, final dissociated CO molecule (C + O atoms), and the CO dissociating transition state, respectively. We tested the corrections of zero-point energies (ZPE) to the adsorption energies of a gaseous CO molecule, the dissociation barriers, and dissociation energies of an adsorbed CO molecule on all six iron surfaces (Supporting Information Table S1). For CO adsorption energy, the maximal correction is 0.06 eV and the average absolute correction is 0.04 eV. For CO dissociation barrier, the maximal correction is 0.04 eV and the average absolute correction is 0.02 eV. For CO dissociation energy, the maximal correction is 0.07 eV and the average absolute correction is 0.05 eV. All these rather small corrections do not alter the results and conclusion without corrections; therefore, we used all energetics without ZPE corrections for our analysis and discussion.

2.2. Models. Calculation of the α-Fe bulk crystal structure with a k-point mesh of 9 × 9 × 9 gives a lattice constant of 2.84 Å and a local spin magnetic moment of 2.214 μ_B, in good agreement with other DFT calculations[55,56] and experiment.[57] For studying CO adsorption on an α-Fe catalyst, apart from the (100) surface in our previous work,[42] other five body-centered cubic (bcc) surfaces are considered: two low-index (110) and (111) surfaces for the basic structures and three high-index (210), (211), and (310) surfaces for the step and kinked structures. Theoretical studies on the surface structures and stability from the literature[58−62] are compiled in Supporting Information Table S2. All these studies show that the (110) and (100) surfaces are most stable, followed by the (211) and (310) surfaces. Depending on the models and methods, the (210) and (111) surfaces have very close surface energies and are less stable.

Different from the models reported in literature, we used much larger surface sizes in our calculations. For (110), a $p(3 \times 4)$ model with three atomic layers was used, and the first layer was allowed to relax. For (111), a $p(2 \times 3)$ model with seven atomic layers was used, and the top three layers were allowed to relax. For (210), a $p(3 \times 2)$ model with six atomic layers was used, and the top four layers were allowed to relax. For (211), a $p(4 \times 2)$ model with four atomic layers was used, and the top two layers were allowed to relax. For (310), a $p(3 \times 2)$ model with six atomic layers was used, and the top three layers were allowed to relax. The k-point mesh of 3 × 3 × 1 was used for all these surfaces. These models have been proved to be reasonable to clearly describe the properties of the corresponding Fe surfaces based on the previous work.[62,63]

2.3. Thermodynamics. As a convenient tool to solve problems referring to real reaction conditions, ab initio atomistic thermodynamics proposed by Scheffler and Reuter[64,65] has been widely and successfully applied in many other systems.[66−73] The detailed description of the method can be found in the Supporting Information.

3. RESULTS AND DISCUSSIONS

3.1. Adsorption Sites. Figure 1 shows the schematic side and top views of the six Fe surfaces along with their possible adsorption sites. The (100) surface has top (T), bridge (B), and 4-fold hollow (4F) sites; (110) has top (T), short-bridge (SB), long-bridge (LB), and 3-fold (3F) sites; (111) has top (T), shallow-hollow (SH), deep-hollow (DH), and 4-fold hollow (4F) sites. On the high-index surfaces, more adsorption sites are available. For example, (210) has 11 adsorption sites: three top (T_1, T_2, T_3), three bridge (B_1, B_2, B_3), four 3-fold ($3F_1$, $3F_2$, $3F_3$, $3F_4$), and one 4-fold (4F) sites. Surface (211) has five adsorption sites: one top (T), one bridge (B), two 3-fold ($3F_1$, $3F_2$), and one 4-fold (4F) sites. Surface (310) also has five adsorption sites: one top (T), one bridge site (B), two 3-fold ($3F_1$, $3F_2$), and one 4-fold (4F) sites.

3.2. Lowest-Coverage CO Adsorption. It is found that not all available adsorption sites can stably adsorb CO at the lowest coverage. The most stable adsorption configurations for one CO molecule on these surfaces are given in Figure 2, and the other less stable configurations are given in the Supporting Information (Figure S1). Table 1 lists the systematically computed CO adsorption energies and dissociation barriers as well as dissociation energies on these surfaces along with all available literature data. It shows clearly that all these computed data are not only different on surfaces but also method- and model-dependent in some cases.

On the Fe(100) surface, the most stable adsorption configurations of one CO molecule is located on the 4-fold site with the C atom coordinating with four surface Fe atoms

dx.doi.org/10.1021/cs500287r | ACS Catal. 2014, 4, 1991−2005

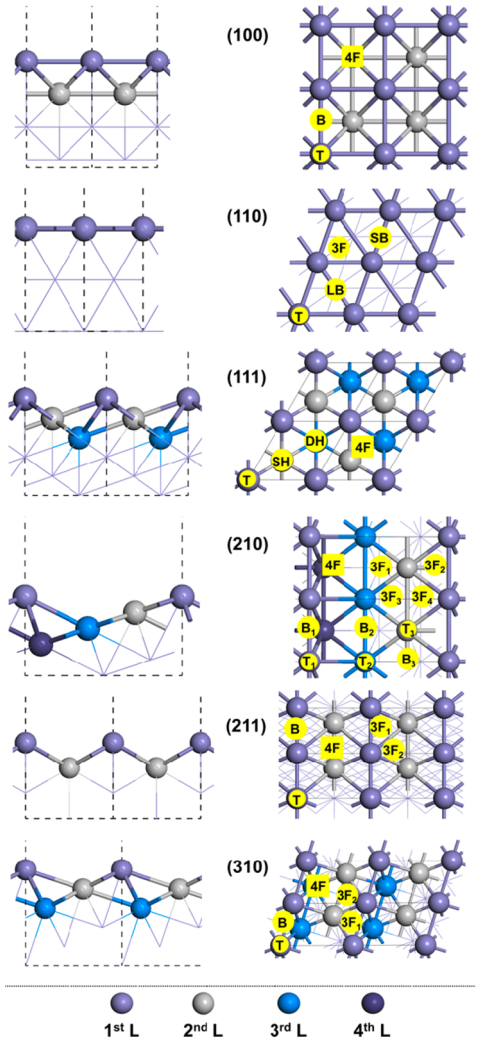

Figure 1. Schematic side and top views of Fe(100), (110), (111), (210), (211), and (310) surfaces and possible adsorption sites.

and the O atom interacting with two surface Fe atoms. The C−O bond length is elongated to 1.32 Å with respect to gaseous CO (1.14 Å), and the computed C−O stretching frequency is 1172 cm^{-1}. The calculated adsorption energy is −2.14 eV.[42] Experimentally, this adsorption configuration is assigned to the α_3 adsorption state from TDS. In addition, we also found stable adsorption configurations at the top (−1.72 eV) and bridge (−1.51 eV) sites. Our computed adsorption energy of the most stable configuration (−2.14 eV) is similar to that (−2.17 eV) by Sorescu et al.[41] because the same software and functional were used. However, the results obtained with RPBE (−1.90 eV[30]), PW91 (−2.02,[30] −2.54 eV[31]), and cluster model (−1.62 eV[29]) are obviously different on the basis of quite different methods and models.

On the Fe(110) surface, the top site forms the most stable CO adsorption configuration with a C−O distance of 1.18 Å and C−O stretching frequency of 1900 cm^{-1}. This most stable adsorption site is the same as that found at low coverage in other studies. Our computed adsorption energy (−1.88 eV) is close to the available data with PW91 (−1.95 eV)[33] and PBE (−1.88,[34] −2.00,[35] −1.88 eV[41]), but higher than those obtained with RPBE (−1.58 eV) and PKZB (−1.67 eV).[34] In addition, we also found stable adsorption configurations at the short bridge (−1.66 eV), the long bridge (−1.81 eV), and the 3-fold capping (−1.81 eV) sites, and they are close to that of the most stable adsorption configuration.

On the Fe(111) surface, the shallow-hollow site with the C atom coordinating with one Fe atom forms the most stable CO adsorption configuration, with a C−O distance of 1.20 Å and C−O stretching frequency of 1739 cm^{-1}. Our computed adsorption energy (−2.13 eV) is similar to that (−2.09 eV) with PBE in a $\sqrt{3} \times \sqrt{3}$ model.[41] A relatively larger difference is found with the results from PBE (−2.45 eV)[36] and RPBE (−2.08 eV).[37] Such differences presumably come from the use of ultrasoft pseudopotential (USPP). In addition, the top (−1.46 eV), the deep-hollow (−1.48 eV), and the 3-fold (−1.98 eV) adsorption configurations are much less stable than the most stable adsorption configuration at the shallow-hollow site.

On the (211) surface, the most stable CO adsorption configuration is the 4-fold site with the C atom coordinating to four Fe atoms and the O atom interacting with one Fe atom, the C−O distance is 1.28 Å, and the C−O stretching frequency is 1274 cm^{-1}. Our adsorption energy (−1.94 eV) is higher than that (−1.72 eV) with PBE[41] using a small super cell. The RPBE[39] value (−1.92 eV) using a small super cell is similar to our result from PBE, but they are not comparable because they used USPP to include the electron−ion interaction. The PW91 value (−2.41 eV) with a small super cell[39] is much higher than those from both PBE and RPBE. In addition, we also found two top (−1.77 and −1.67 eV) and one bridge (−1.78 eV) adsorption configurations, and they are less stable than the most stable adsorption configuration at the 4-fold site.

On the (310) surface, the most stable CO adsorption configuration is the 4-fold site with the C atom coordinating

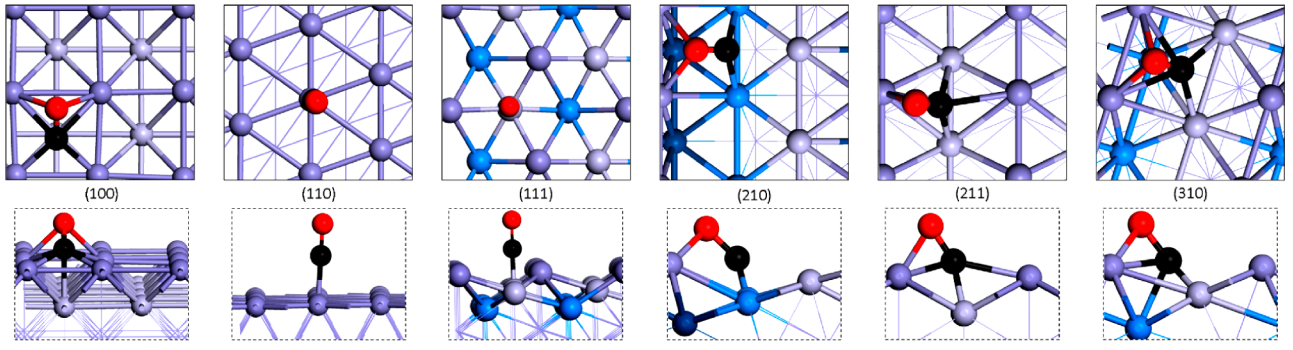

Figure 2. Structures of the most stable CO adsorption configurations on six iron surfaces (black ball, C; red ball, O; the other balls for Fe in different layers).

dx.doi.org/10.1021/cs500287r | ACS Catal. 2014, 4, 1991−2005

Table 1. Adsorption Energies (E_{ads}), Dissociation Barriers (E_a), and Dissociation Energies (E_r) of the Most Stable CO Adsorption Configuration As Well As the C−O Stretching Frequencies (υ_{CO}), the C−O Distances (R) in the Adsorbed Initial States (IS), and Dissociating Transition States (TS) on Six Iron Surfaces

E_{ads}, eV	E_a, eV	E_r[a], eV	υ_{CO}, cm^{-1}	R_{C-O} (IS), Å	R_{C-O} (TS), Å	ref
			(100)			
−1.62 (cluster)				1.30		29
−2.02 (PW91, 2 × 2)	1.06		1246	1.32		30
−1.90 (RPBE, 2 × 2)				1.32		30
−2.54 (PW91, 2 × 2)	1.14		1158	1.32		31
−2.17 (PBE, 2 × 2)	1.07		1189	1.32	1.93	41
−2.14 (PBE, 3 × 4)	1.03	−0.93 (−1.20)	1172	1.32	1.93	42
			(110)			
−1.88 (PBE, 3 × 4)	1.51	−0.46 (−0.74)	1900	1.18	1.75	this work
−1.95 (PW91, 2 × 2)				1.16		33
−1.88 (PBE, 2 × 2)	1.52		1928		1.74	34
−1.58 (RPBE, 2 × 2)						34
−1.67 (PKZB, 2 × 2)						34
−2.00 (PBE, 2 × 2)				1.17		35
−1.88 (PBE, 2 × 2)	1.52				1.74	41
			(111)			
−2.13 (PBE, 2 × 3)	1.17	0.06 (−0.09)	1739	1.20	1.85	this work
−2.45 (PBE, $\sqrt{3} \times \sqrt{3}$)	1.39			1.19		36, 37
−2.08 (RPBE, $\sqrt{3} \times \sqrt{3}$)	1.53				2.00	37
−2.09 (PBE, $\sqrt{3} \times \sqrt{3}$)	1.20				1.80	41
			(210)			
−2.00 (PBE, 3 × 2)	1.11	−0.32 (−0.82)	1115	1.33	1.97	this work
			(211)			
−1.94 (PBE, 4 × 2)	1.06	−0.20 (−0.39)	1274	1.28	1.95	this work
−2.41 (PW91, 2 × 1)	0.78			1.28	1.83	39
−1.92 (RPBE, 2 × 1)	0.93					39
−1.72 (PBE, 2 × 2)	1.02			1.28	1.93	41
			(310)			
−2.13 (PBE, 3 × 2)	0.98	−0.39 (−1.07)	1104	1.33	1.93	this work
−1.85 (PW91, 2 × 1)	0.94		1147	1.33	1.80	40
−2.10 (PBE, 2 × 2)	0.91		1134	1.33		41

[a]Dissociation energy in parentheses is related to the most stable adsorbed C and O atoms after diffusion.

with four Fe atoms and the O atom interacting with two surface Fe atoms. The C−O distance is 1.33 Å, and the C−O stretching frequency is 1104 cm^{-1}. Our computed adsorption energy (−2.13 eV) is close to the reported PBE-$p(2 \times 2)$[41] value (−2.10 eV) because the same software and functional were used. A relative smaller value (−1.85 eV[40]) was reported by using USPP and PW91 as well as a small supercell $p(2 \times 1)$, which may overestimate the lateral repulsive interaction. In addition, we also found two tilted top (−1.60 and −1.79 eV) and one 4-fold (−1.72 eV) adsorption configurations, and they are much less stable than the most stable adsorption configuration at the 4-fold site.

On the (210) surface, the most stable adsorption configuration is the 4-fold site with the C atom coordinating with two deep-layer Fe atoms and the O atom interacting with two surface Fe atoms with a C−O distance of 1.33 Å and CO stretching frequency of 1115 cm^{-1}. We also found two top (−1.69 and −1.74 eV) and three 3-fold (−1.70, −1.72, and −1.63 eV) adsorption configurations, and they are much less stable than the most stable adsorption configuration at the 4-fold site (−2.00 eV). Because no theoretical studies about CO adsorption on this surface are available, no comparison with our data can be made.

Although CO interaction on iron single crystalline surfaces has been intensively studied in recent decades, a general and critical comparison among the results obtained with different models and methods is neither easy nor straightforward.[74] At first, the lowest coverage for different surface sizes indeed represents different coverage, and reducing the surface size to create high coverage is not a reasonable choice. Generally, models with larger surface sizes show stronger adsorption than models with smaller surface sizes, and this is probably due to the difference in lateral repulsive interaction. As summarized in Table 1, PBE gives higher adsorption energies than the RPBE, and this is due to the intrinsic properties of these methods. In addition, different methods for solving electron−ion and electron−electron interactions as well as basis sets also give different results. It is noted that different computational parameters can also result in quite different results. However, it is reported that different methods and functional on the basis of the same surface model can give very close structural as well as kinetic and thermodynamic parameters. For example, PAW−PBE and USPP−PW91 with VASP, and USP−PBE and USPP−PW91 with CASTEP to calculate the hydrogenation and the respective C−C coupling reactions of carbon species on the $Fe_5C_2(001)$ surface.[75]

In contrast, our results enable a direct and systematic comparison in CO adsorption at low coverage. On the (100), (111), and (310) surfaces, the most stable adsorption configurations have almost identical adsorption energies, but

dx.doi.org/10.1021/cs500287r | ACS Catal. 2014, 4, 1991−2005

the adsorbed CO is more strongly activated on the (100) and (310) surfaces than on the (111) surface on the basis of the computed C−O distances (1.32 and 1.33 vs 1.18 Å, respectively) or the CO-stretching frequencies (1172 and 1104 vs 1793 cm^{-1}, respectively), although CO has moderate adsorption energies (−2.00 and −1.94 eV, respectively) on the (210) and (211) surfaces, but it is highly activated on the basis of the computed C−O distances (1.33 and 1.28 Å, respectively) or C−O stretching frequencies (1144 and 1273 cm^{-1}, respectively). On the most stable (110) surface, CO has not only the lowest adsorption energy (−1.88 eV), but also the weakest activation with a C−O distance and stretching frequency of 1.18 Å and 1900 cm^{-1}.

3.3. High Coverage CO Adsorption. To discuss the coverage effects of CO adsorption and activation on iron surfaces, it is necessary to find the stable adsorption configurations and energies at different coverages on each surface. As referred to in the Methods section, the computed stepwise adsorption energies (ΔE_{ads}) are applied to get the saturated coverage. The structures and energies (ΔE_{ads}) of the most stable adsorption sites for stepwise CO adsorption are given in the Supporting Information (Figures S2−S6).

On the (100) surface,[42] the first four adsorbed CO molecules (n_{CO} = 1−4) have the 4-fold adsorption configuration and very similar adsorption energies, indicating their negligible lateral repulsive interaction and their independence. At n_{CO} = 5−8, lateral repulsive interaction of the adsorbed CO molecules becomes significant and affects the value of ΔE_{ads}, but all the adsorbed CO molecules still have the 4-fold adsorption configuration. At n_{CO} = 9, the bridge adsorption configuration appears, and one bridge and eight 4-fold adsorption configurations coexist. At n_{CO} = 10, there are three bridge and seven 4-fold adsorption configurations. At the saturated coverage (n_{CO} = 11), there are one top, three bridge, and seven 4-fold adsorption configurations.

On the (110) surface (Supporting Information Figure S2), the top adsorption configuration is the most stable at low coverage, and the first three CO molecules (n_{CO} = 1−3) have the same adsorption configuration and similar stepwise adsorption energies. At n_{CO} = 4, the most stable adsorption configuration changes from the top sites to the long bridge sites, and all four CO molecules have the same adsorption configuration. At n_{CO} > 4, the 3-fold hollow and short bridge configurations appear. At the saturated coverage (n_{CO} = 8), three adsorption configurations (short bridge, long bridge, and 3-fold hollow) coexist on the surface, and the top adsorption configuration disappeared.

On the (111) surface (Supporting Information Figure S3), the shallow hollow adsorption configuration is most stable at low coverage, and the first six CO molecules (n_{CO} = 1−6) have the same adsorption mode and also very similar stepwise adsorption energies. At n_{CO} = 7, the qusi-4-fold adsorption configuration appears, and the stepwise adsorption energy decreases. At the saturated coverage (n_{CO} = 9), three adsorption configurations (top, shallow hollow and qusi-4-fold) coexist on the surface.

On the (210) surface (Supporting Information Figure S4), the most stable adsorption configuration is located at the 4-fold hollow site with n_{CO} < 6, and the top adsorption configuration appears at n_{CO} = 7. At the saturated coverage (n_{CO} = 12), two adsorption configurations coexist (top and 4-fold hollow sites). On the (211) surface (Supporting Information Figure S5), the most stable adsorption configuration is located in the 4-fold hollow site at low coverage, and the top and bridge adsorption configurations appear with coverage increase. At the saturated coverage (n_{CO} = 10), the coexistence of top, bridge, and 4-fold adsorption configurations become possible. On the (310) surface (Supporting Information Figure S6), the most stable adsorption configuration is located in the 4-fold hollow site at low coverage, and the 3-fold hollow adsorption configuration appears at n_{CO} > 7. The saturated coverage with nine CO molecules (n_{CO} = 9) has bridge and 4-fold hollow adsorption configurations.

3.4. CO Dissociation. On the basis of the most stable CO molecular adsorption configurations, we also computed CO dissociation at different coverage. The structures of the corresponding initial states (IS), transition states (TS), and final states (FS) at the lowest coverage are shown in Figure 3. Table 1 lists the computed CO dissociation barriers and the critical C−O distances along with the available literature data for comparison.

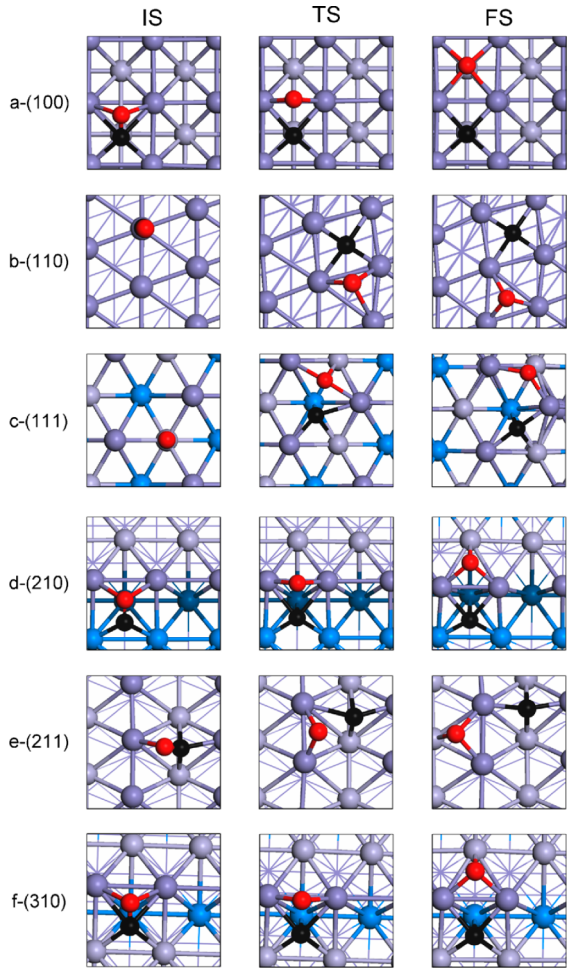

Figure 3. Initial state (IS), transition state (TS), and final state (FS) of CO dissociation from most stable adsorption sites on six iron surfaces (black ball, C; red ball, O; the other balls for Fe in different layers).

3.4.1. Lowest-Coverage CO Dissociation. As shown in Table 1, the CO dissociation barriers on the (310), (100), (211), and (210) surfaces (0.98, 1.03, 1.06, and 1.11 eV, respectively) are lower than those on the (111) and (110) surfaces (1.17 and 1.51 eV, respectively). This indicates that the CO dissociation barrier does not correlate with the surface

dx.doi.org/10.1021/cs500287r | ACS Catal. 2014, 4, 1991−2005

stability (Supporting Information Table S2) because of their different initial and most stable adsorption configurations. Despite the differences in methods (PBE and PW91) and models, the computed C−O dissociation barriers on the (100) surface are very close, and the same trend is also found on the (110) surface. On the (111) surface, however, PBE gives different CO dissociation barriers because of different transition state structures, and RPBE gives a higher CO dissociation barrier than PBE by using the same transition state structure. On the (211) surface, PBE gives a higher CO dissociation barrier than PW91 because of different transition state structures, and RPBE gives a higher CO dissociation barrier than PW91 by using the same transition state structures. On the (310) surface, different methods give different transition state structures and different dissociation barriers; however, no reported data for CO dissociation on the (210) surface are available for comparison.

On the basis of the computed dissociation barriers for the most stable adsorption configurations and the computed dissociation energies for the most stable coadsorbed C and O atoms (diffusion after dissociation), we checked their Brønsted−Evans−Polanyi (BEP) relation (Figure 4). In contrast to the perfect linear BEP relation for N_2 dissociation on the same surface having the same adsorption site and the similar transition state distances over a range of pure metals with face-centered cubic crystal structures (i.e., M(211), M = Mn, Fe, Co, Ni, Cu, Mo, Ru, Rh, Pd, Ag, Ir, Pt, Au, W, and Re)[76] as well as for CO dissociation on a set of transition metals with the same or similar surface structures (i.e., Ru(0001), Rh(111), and Pd(111) as well as Os(0001), Ir(111), and Pt(111) surface),[77−79] there is no such correlation for CO dissociation on these different iron surfaces, and the correlation coefficient is miserably low (R = 0.25). This is due to their large geometric differences in the IS, TS, and FS, that is, the structures of the initial state (IS) and final state (FS) represent the thermodynamically most stable molecular and dissociative adsorption configurations on each surface, respectively, and their adsorption configurations differ from surface to surface as a result of their intrinsic surface structures. For example, the most stable CO adsorption configurations are located on 4-fold hollow sites on the (100), (210), (211), and (310) surfaces with the C atom in CO coordinating with many surface Fe atoms, whereas those on the (110) and (111) surfaces are located on the top sites with the C atom in CO coordinating with only one surface Fe atom. All of these differences in surface structures and CO adsorption configurations on each surface result in quite different structures of the transition and final states.

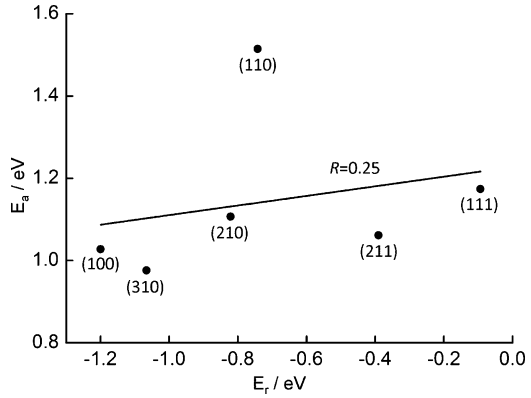

Figure 4. Correlation between CO dissociation barriers and dissociation energies.

3.4.2. High Coverage CO Dissociation. Apart from our recent study of high-coverage CO activation on the Fe(100) surface,[42] most theoretical studies of CO adsorption and dissociation on iron surfaces (Table 1) have been carried out at the lowest coverage and ideal condition. Because the available experimental adsorption or desorption energies are the average of a set of molecules in different adsorption configurations instead of a single molecule (especially at low temperature and high coverage), a direct comparison between theory and experiment is very difficult. A reasonable way to make such a direct comparison between theory and experiment in adsorption or desorption as well as dissociation properties is to include the boundary conditions, such as temperature, pressure, and coverage, in model calculation. Following the same pattern as in our previous work, we further studied CO dissociation at different coverages on another five iron surfaces and included the results on Fe(100) for comparison.

(a) Fe(100). In our previous work, we reported the CO adsorption and desorption as well as dissociation on Fe(100).[42] Our results show that only dissociative adsorption is possible for n_{CO} = 1 and 2. For n_{CO} = 3−7, the surface adsorption states have possible equilibrium between molecular and dissociative CO adsorptions. For n_{CO} = 8−11, only molecular CO adsorption can be found.

(b) Fe(110). For n_{CO} = 1 (Table 2), the computed CO dissociation barrier is lower than its desorption energy (1.51 vs 1.88 eV), and CO dissociation is exothermic by 0.46 eV, indicating that CO dissociation is favorable both kinetically and thermodynamically. The final adsorption state has only dissociative CO adsorption at this coverage.

Table 2. CO Stepwise Dissociation Barriers (E_a), Desorption Energies (ΔE_{des}), and Dissociation Energies (ΔE_{dis}) at Different Coverages on the Fe(110) Surface

nCO	pathways	E_a, eV	ΔE_{des}, eV	ΔE_{dis}, eV
1CO	1CO → 1C + 1O	1.51	1.88	−0.46
2CO	2CO → 1CO + 1C + 1O	1.48	1.86	−0.44
	1CO + 1C + 1O → 2C + 2O	1.71	1.81	+0.07
3CO	3CO → 2CO + 1C + 1O	1.57	1.82	−0.17
	2CO + 1C + 1O → 1CO + 2C + 2O	1.59	1.52	+0.24
	1CO + 2C + 2O → 3C + 3O	1.75	1.60	+1.13
4CO	4CO → 3CO + 1C + 1O	1.53	1.67	−0.24
	3CO + 1C + 1O → 2CO + 2C + 2O	2.62	1.46	+0.24
5CO	5CO → 4CO + 1C + 1O	1.70	1.56	−0.44

For n_{CO} = 2, the dissociation barrier of the first CO molecule is lower than its desorption energy (1.48 vs 1.86 eV), and CO dissociation is exothermic by 0.44 eV, indicating that first CO dissociation is favorable both kinetically and thermodynamically. For the second CO molecule, the dissociation barrier is only slightly lower than own desorption energy (1.71 vs 1.81 eV), and the dissociation becomes slightly endothermic (0.07 eV). Considering the recombinative reaction barrier of 1.64 eV, the second adsorbed CO might have equilibrium between molecular and dissociative adsorptions; therefore, the final adsorption state might have CO + C + O and 2C + 2O in equilibrium on the surface at this coverage.

dx.doi.org/10.1021/cs500287r | ACS Catal. 2014, 4, 1991−2005

For n_{CO} = 3, the dissociation barrier of the first CO molecule is lower than its desorption energy (1.57 vs 1.82 eV), and CO dissociation is exothermic by 0.17 eV; however, the dissociation barriers of the second and third CO molecules (1.59 and 1.75 eV) are higher than their corresponding desorption energies (1.52 and 1.60 eV), and the dissociation is endothermic by 0.24 and 1.13 eV, respectively. This indicates that the second and third CO molecules prefer desorption from the surface instead of dissociation on the surface. The final adsorption state has two adsorbed CO molecules as well as one C and one O atom (2CO + C + O) on the surface.

For n_{CO} = 4, the dissociation barrier of the first CO molecule is lower than its desorption energy (1.53 vs 1.67 eV), and the dissociation is exothermic by 0.24 eV. The dissociation barrier of the second CO molecule is much higher than its own desorption energy (2.62 vs 1.46 eV), and the dissociation is endothermic by 0.24 eV. This indicates that only one CO can dissociate at this coverage, and the final adsorption state has three adsorbed CO molecules as well as one C and one O atom (3CO + C + O) on the surface.

For n_{CO} = 5, the dissociation barrier of the first CO molecule is higher than its desorption energy (1.71 vs 1.56 eV). Therefore, at this coverage, the first step should be CO desorption instead of dissociation, despite the exothermic dissociation (−0.44 eV). The final adsorption state has five adsorbed CO molecules. It can be expected that at high coverage (n_{CO} = 5−8), only desorption is possible because of the very low desorption energies. The final adsorption states have only molecular CO adsorption.

(c) Fe(111). For n_{CO} = 1 (Table 3), the CO dissociation barrier is much lower than its desorption energy (1.17 vs 2.13 eV), and the dissociation process is slightly exothermic by 0.09 eV, indicating that CO dissociation is favorable kinetically but thermodynamically neutral. Considering the recombinative reaction barrier of 1.26 eV, the adsorbed CO molecule might have equilibrium between molecular and dissociative adsorptions. The final adsorption state might have equilibrium between molecular (CO) and dissociative (C + O) adsorptions.

Table 3. CO Stepwise Dissociation Barriers (E_a), Desorption Energies (ΔE_{des}), and Dissociation Energies (ΔE_{dis}) at Different Coverages on the Fe(111) Surface

*n*CO	pathways	E_a, eV	ΔE_{des}, eV	ΔE_{dis}, eV
1CO	1CO → 1C + 1O	1.17	2.13	−0.09
2CO	2CO → 1CO + 1C + 1O	1.13	2.12	−0.14
	1CO + 1C + 1O → 2C + 2O	1.14	2.16	+0.14
3CO	3CO → 2CO+1C+1O	1.27	2.12	+0.14
	2CO+1C + 1O → 1CO + 2C + 2O	1.20	2.16	+0.10
	1CO + 2C + 2O → 3C + 3O	1.02	2.06	−0.02
4CO	4CO → 3CO + 1C + 1O	1.27	2.11	+0.11
	3CO + 1C + 1O → 2CO + 2C + 2O	0.97	2.12	−0.18
	2CO + 2C + 2O → 1CO + 3C + 3O	1.97	2.13	+1.46
	1CO + 3C + 3O → 4C + 4O	2.07	1.74	+1.02
5CO	5CO → 4CO + 1C + 1O	1.23	2.12	+0.16
	4CO + 1C + 1O → 3CO + 2C + 2O	1.97	2.06	+1.18
6CO	6CO → 5CO + 1C + 1O	2.70	2.10	+1.19

For n_{CO} = 2, the dissociation barriers of both CO molecules (1.13 and 1.14 eV) are much lower than their corresponding desorption energies (2.12 and 2.16 eV), and the dissociation of the first CO molecule is exothermic by 0.14 eV, whereas that of the second CO molecule becomes endothermic by 0.14 eV. Considering their recombinative reaction barriers of 1.27 and 1.00 eV, the adsorbed CO molecules might have equilibrium between molecular and dissociative adsorption. The final adsorption state might have possible equilibrium between molecular (2CO) and dissociative (2C + 2O) adsorptions.

For n_{CO} = 3, the dissociation barriers (1.27, 1.20, and 1.02 eV) of all three CO molecules are much lower than their corresponding desorption energies (2.12, 2.16, and 2.06 eV), and the dissociation of the first two CO molecules is slightly endothermic by 0.14 and 0.10 eV, respectively, whereas that of the third CO becomes thermoneutral. Considering their recombinative reaction barriers of 1.13, 1.30, and 1.04 eV, the adsorbed CO molecules might have equilibrium between molecular (3CO) and dissociative (3C + 3O) adsorption. The final adsorption state might have possible equilibrium between molecular (3CO) and dissociative (3C + 3O) adsorptions.

For n_{CO} = 4, the dissociation barriers of the first two CO molecules (1.27 and 0.97 eV) are lower than their desorption energies (2.11 and 2.12 eV), and the dissociation of the first CO is endothermic by 0.11 eV, whereas that of the second one is exothermic by 0.18 eV. For the dissociation of the third CO molecule, this process is very endothermic (1.46 eV), although the barrier is lower than the desorption energy (1.97 vs 2.13 eV). Considering the very low recombinative reaction barriers of 0.51 eV, the third CO molecule prefers molecular instead of dissociative adsorption. The dissociation barrier of the fourth CO molecule (2.07 eV) is higher than its desorption energy (2.07 vs 1.74 eV), and the dissociation is endothermic by 1.02 eV. The fourth CO molecule prefers desorption instead of dissociation. The final adsorption state might predominately have 2CO + 2C + 2O on the surface at this coverage.

For n_{CO} = 5, the dissociation barrier of the first CO molecule is much lower than its desorption energy (1.23 vs 2.12 eV), and the dissociation process is endothermic by 0.16 eV. Considering the low recombinative reaction barriers of 1.07 eV, the first CO molecule might have an equilibrium between molecular and dissociative adsorption, although the dissociation barrier of the second CO is similar to its desorption energy (1.97 vs 2.06 eV), but this process is highly endothermic (1.18 eV), and the recombinative reaction is more favorable. Consequently, the final adsorption state might have 5CO and 4CO + C + O in equilibrium.

For n_{CO} = 6, the dissociation barrier of the first CO is 2.70 eV, which is higher than its desorption energy (2.10 eV), and this process is highly endothermic by 1.19 eV. Therefore, CO prefers desorption instead of dissociation. It is to be expected that at coverage of n_{CO} = 6−9, the final adsorption states have only molecular CO adsorption.

(d) Fe(210). For n_{CO} = 1−5 (Table 4), the computed CO dissociation barriers are much lower than their desorption energies, and the dissociation is exothermic for all adsorbed CO molecules, indicating that CO dissociation is favorable both kinetically and thermodynamically at each coverage. The final adsorption state is only dissociative (*n*C + *n*O) on the surface.

For n_{CO} = 6, the dissociation barrier of the first CO molecule is close to its desorption energy (1.58 vs 1.69 eV), and the dissociation is slightly exothermic (−0.08 eV). This indicates a possible equilibrium among molecular adsorption and desorption as well as dissociative adsorption. However, it should be noted that for the other five adsorbed CO molecules, the dissociation barriers are lower than their desorption

dx.doi.org/10.1021/cs500287r | ACS Catal. 2014, 4, 1991−2005

Table 4. CO Stepwise Dissociation Barriers (E_a), Desorption Energies (ΔE_{des}), and Dissociation Energies (ΔE_{dis}) at Different Coverages on the Fe(210) Surface

*n*CO	pathways	E_a, eV	ΔE_{des}, eV	ΔE_{dis}, eV
1CO	1CO → 1C + 1O	1.11	2.00	−0.32
2CO	2CO → 1CO + 1C + 1O	1.11	2.00	−0.21
	1CO + 1C + 1O → 2C + 2O	1.07	1.89	−0.27
3CO	3CO → 2CO + 1C + 1O	1.12	1.92	−0.22
	2CO + 1C + 1O → 1CO + 2C + 2O	1.26	1.93	−0.21
	1CO + 2C + 2O → 3C + 3O	1.11	1.87	−0.40
4CO	4CO → 3CO + 1C + 1O	1.29	1.97	−0.15
	3CO + 1C + 1O → 2CO + 2C + 2O	1.17	1.88	−0.34
	2CO + 2C + 2O → 1CO + 3C + 3O	1.28	1.88	−0.19
	1CO + 3C + 3O → 4C + 4O	1.05	1.83	−0.47
5CO	5CO → 4CO + 1C + 1O	1.26	1.69	−0.14
	4CO + 1C + 1O → 3CO + 2C + 2O	1.12	1.87	−0.36
	3CO + 2C + 2O → 2CO + 3C + 3O	1.58	1.70	−0.14
	2CO + 3C + 3O → 1CO + 4C + 4O	1.22	1.65	−0.40
	1CO + 4C + 4O → 5C + 5O	1.24	1.59	−0.10
6CO	6CO → 5CO + 1C + 1O	1.58	1.69	−0.08
	5CO + 1C + 1O → 4CO + 2C + 2O	1.28	1.63	−0.29
	4CO + 2C + 2O → 3CO + 3C + 3O	1.23	1.56	−0.15
	3CO + 3C + 3O → 2CO + 4C + 4O	1.56	1.59	−0.15
	2CO + 4C + 4O → 1CO + 5C + 5O	1.18	1.57	−0.39
	1CO + 5C + 5O → 6C + 6O	1.08	1.60	−0.20
7CO	7CO → 6CO + 1C + 1O	1.56	1.57	−0.11
	6CO + 1C + 1O → 5CO + 2C + 2O	1.25	1.59	−0.30
	5CO + 2C + 2O → 4CO + 3C + 3O	1.12	1.60	−0.07
	4CO + 3C + 3O → 3CO + 4C + 4O	1.52	1.52	−0.15
	3CO + 4C + 4O → 2CO + 5C + 5O	1.27	1.52	−0.26
	2CO + 5C + 5O → 1CO + 6C + 6O	1.39	1.39	+0.68
8CO	8CO → 7CO + 1C + 1O	1.53	1.57	−0.04
	7CO + 1C + 1O → 6CO + 2C + 2O	1.57	1.61	−0.13
	6CO + 2C + 2O → 5CO + 3C + 3O	1.30	1.59	−0.08
	5CO + 3C + 3O → 4CO + 4C + 4O	1.26	1.54	−0.16
9CO	9CO → 8CO + 1C + 1O	1.58	1.45	−0.04

energies, and the dissociation processes are exothermic. These steps are very similar to those for n_{CO} = 5. The final adsorption state is only dissociative (6C + 6O) on the surface.

For n_{CO} = 7, the dissociation barrier of the first CO molecule is close to its desorption energy (1.56 vs 1.67 eV), and the dissociation is slightly exothermic (−0.11 eV). This indicates a possible equilibrium among molecular adsorption, desorption, and dissociative adsorption. After dissociation of the first CO molecule, the second and third adsorbed CO molecules favor dissociation instead of desorption, and the dissociation is slightly exothermic. After dissociation of the first three adsorbed CO molecules, the fourth adsorbed CO molecule has a possible equilibrium among molecular adsorption, desorption, and dissociative adsorption. On the basis of the first four dissociative CO adsorptions, the fifth adsorbed CO molecule favors exothermic dissociation. For the sixth adsorbed CO molecule, the dissociation barrier is equal to its desorption energy, and the dissociation becomes highly endothermic. It is to be expected that the seventh adsorbed CO molecule will desorb instead of dissociate. The final adsorption state might have 2CO + 5C + 5O on the surface at this coverage.

For n_{CO} = 8, the same situation has been found as for n_{CO} = 6 and 7. The first CO molecule might have possible equilibrium among molecular adsorption, desorption, and dissociative adsorption on the basis of the computed dissociation barrier (1.53 eV), desorption energy (1.57 eV), and dissociation energy (−0.04 eV). After the dissociation of the first CO molecule, the subsequent three adsorbed CO molecules might have equilibrium between molecular and dissociative adsorption on the surface at this coverage. It is to be expected that the fifth adsorbed CO molecule will desorb instead of dissociate. The final adsorption state might have 4CO + 4C + 4O on the surface at this coverage.

For n_{CO} = 9, the dissociation barrier of the first adsorbed CO molecule is larger than its desorption energy (1.58 vs 1.45 eV), indicating the preference of desorption over dissociation. At n_{CO} = 9−12, only molecular adsorption is possible.

(e) Fe(211). For n_{CO} = 1−2 (Table 5), the computed CO dissociation barriers are much lower than their desorption

Table 5. CO Stepwise Dissociation Barriers (E_a), Desorption Energies (ΔE_{des}), and Dissociation Energies (ΔE_{dis}) at Different Coverages on the Fe(211) Surface

*n*CO	pathways	E_a, eV	ΔE_{des}, eV	ΔE_{dis}, eV
1CO	1CO → 1C + 1O	1.06	1.94	−0.20
2CO	2CO → 1CO + 1C + 1O	1.05	1.92	−0.22
	1CO + 1C + 1O → 2C + 2O	1.03	1.93	−0.14
3CO	3CO → 2CO + 1C + 1O	1.02	1.92	−0.29
	2CO + 1C + 1O → 1CO + 2C + 2O	1.30	1.94	+0.22
	1CO + 2C + 2O → 3C + 3O	1.94	1.92	+1.01
4CO	4CO → 3CO + 1C + 1O	1.29	1.92	+0.09
	3CO + 1C + 1O → 2CO + 2C + 2O	1.30	1.91	+0.73
	2CO + 2C + 2O → 1CO + 3C + 3O	1.92	1.75	+1.02
5CO	5CO → 4CO + 1C + 1O	1.44	1.62	+0.40
	4CO + 1C + 1O → 3CO + 2C + 2O	1.72	1.67	+0.61
	3CO + 2C + 2O → 2CO + 3C + 3O	1.79	1.43	+0.90
6CO	6CO → 5CO + 1C + 1O	1.10	1.37	+0.22
	5CO + 1C + 1O → 4CO + 2C + 2O	1.75	1.54	+0.92
7CO	7CO → 6CO + 1C + 1O	1.43	1.06	+0.59
8CO	8CO → 7CO + 1C + 1O	1.92	1.57	+0.65

energies, and the dissociation is exothermic for all adsorbed CO molecules, indicating that CO dissociation is favorable both kinetically and thermodynamically. The final adsorption state is only dissociative on the surface.

For n_{CO} = 3, the dissociation barrier of the first CO molecule is lower than its own desorption energy (1.02 vs 1.92 eV), and the dissociation is exothermic (−0.29 eV). The first CO dissociation is favorable both kinetically and thermodynamically. Although the dissociation barrier of the second CO molecule is lower than its desorption energy (1.30 vs 1.94 eV), the dissociation is endothermic (0.22 eV), and the recombinative reaction becomes more favorable. For the third CO molecule, the dissociation barrier comes very close to its desorption energy (1.94 vs 1.92 eV), and the dissociation is highly endothermic (1.01 eV). Therefore, the final adsorption state might predominantly have 2CO + C + O on the surface at this coverage.

For n_{CO} = 4, the dissociation barrier of the first CO molecule is lower than its desorption energy (1.29 vs 1.92 eV), and the dissociation is slightly endothermic (0.09 eV). Considering the low recombinative reaction barrier of 1.20 eV, the first CO molecule might have equilibrium between molecular and dissociative adsorption. Although the dissociation barrier of the second CO molecule is lower than its desorption energy

dx.doi.org/10.1021/cs500287r | ACS Catal. 2014, 4, 1991−2005

(1.30 vs 1.91 eV), the dissociation process is strongly endothermic (0.73 eV), and the recombinative reaction becomes more favorable. For the third CO molecule, the dissociation barrier becomes higher than its desorption energy (1.92 vs 1.75 eV), and the dissociation is highly endothermic (1.02 eV). Consequently, the final adsorption state might have 4CO and 3CO + C + O in equilibrium on the surface at this coverage.

For n_{CO} = 5 and 6, although the dissociation barriers of the first CO molecules are lower than their own desorption energies, the dissociation processes are strongly endothermic, indicating that a molecular instead of dissociative adsorption is more favorable. For the second and third CO molecules, the dissociation barriers become higher than their desorption energy, and the dissociation is strongly endothermic. Therefore, the final adsorption state most likely has 5CO on the surface at this coverage. For n_{CO} = 7 and 8, the dissociation barriers of the first adsorbed CO molecule are larger than their desorption energy (1.58 vs 1.45 eV), indicating a preference for desorption over dissociation. At n_{CO} = 5−10, therefore, only molecular adsorption is possible.

(f) Fe(310). For n_{CO} = 1 (Table 6), the lower CO dissociation barrier than its own desorption energy (0.98 vs 2.13 eV) and the exothermic dissociation reaction (−0.38 eV) indicate that CO dissociation is favorable both kinetically and thermodynamically. The final adsorption state is only dissociative on the surface.

Table 6. CO Stepwise Dissociation Barriers (E_a), Desorption Energies (ΔE_{des}), and Dissociation Energies (ΔE_{dis}) at Different Coverages on the Fe(310) Surface

*n*CO	pathways	E_a, eV	ΔE_{des}, eV	ΔE_{dis}, eV
1CO	1CO → 1C + 1O	0.98	2.13	−0.38
2CO	2CO → 1CO + 1C + 1O	1.06	2.19	−0.05
	1CO + 1C + 1O → 2C + 2O	1.05	1.86	+0.05
3CO	3CO → 2CO + 1C + 1O	1.13	2.05	+0.01
	2CO + 1C + 1O → 1CO + 2C + 2O	1.22	1.73	+0.10
	1CO + 2C + 2O → 3C + 3O	0.96	1.93	−0.30
4CO	4CO → 3CO + 1C+1O	1.31	2.09	+0.08
	3CO + 1C + 1O → 2CO + 2C + 2O	1.12	2.03	−0.01
	2CO + 2C + 2O → 1CO + 3C + 3O	1.16	1.57	+0.04
	1CO + 3C + 3O → 4C + 4O	1.00	1.79	−0.08
5CO	5CO → 4CO + 1C + 1O	1.44	1.82	+0.42
	4CO + 1C + 1O → 3CO + 2C + 2O	1.22	1.76	+0.16
	3CO + 2C + 2O → 2CO + 3C + 3O	1.35	1.42	−0.02
	2CO + 3C + 3O → 1CO + 4C + 4O	1.22	1.38	+0.03
	1CO + 4C + 4O → 5C + 5O	1.03	1.28	−0.22
6CO	6CO → 5CO + 1C + 1O	1.72	1.86	+0.55
	5CO + 1C + 1O → 4CO + 2C + 2O	1.39	1.81	+0.29
	4CO + 2C + 2O → 3CO + 3C + 3O	1.23	1.35	+0.06
	3CO + 3C + 3O → 2CO + 4C + 4O	1.40	1.42	+0.14
	2CO + 4C + 4O → 1CO + 5C + 5O	1.17	1.22	−0.14
	1CO + 5C + 5O → 6C + 6O	0.91	1.32	−0.36
7CO	7CO → 6CO + 1C + 1O	1.53	0.56	−0.16

For n_{CO} = 2, the dissociation barriers of both CO molecules are lower than their desorption energies, and the dissociation processes are almost thermoneutral. Considering their low recombinative reaction barriers of 1.10 and 1.00 eV, both CO molecules might have equilibrium between molecular and dissociative CO adsorptions.

For n_{CO} = 3, the behavior of the first two CO molecules mimics those for n_{CO} = 2, and they might have equilibrium between molecular and dissociative CO adsorption; however, it should be noted that for the third adsorbed CO molecule, the dissociation barrier is lower than its own desorption energies (1.58 vs 1.69 eV), and the dissociation process becomes exothermic (−0.30 eV). The final adsorption state should be only dissociative on the surface at this coverage.

For n_{CO} = 4, the barriers for all stepwise dissociations are lower than their desorption energies, and the dissociation processes are nearly thermoneutral. Considering their recombinative barriers, the final adsorption state might have equilibrium between molecular and dissociative CO adsorptions.

For n_{CO} = 5, the barriers for all stepwise dissociation are lower than their desorption energies, and the dissociation processes are endothermic for the first two CO molecules and nearly thermoneutral for the last three CO molecules. This indicates the preferable molecular adsorption for the first two CO molecules and equilibrium between molecular and dissociative adsorption for the last three CO molecules. The final adsorption state might have equilibrium between molecular and dissociative CO adsorptions. Similar results have been found for n_{CO} = 6. However, for n_{CO} = 7, desorption is more favorable than dissociation for the first CO molecule. Therefore, for n_{CO} = 7−9, only molecular CO adsorption is possible.

3.5. CO Stable Coverage and Adsorption States with Temperature and Pressure. On the basis of our identified molecular and dissociative CO adsorption states at different coverage, the effects of temperature and pressure on CO adsorption and activations can be estimated by applying ab initio thermodynamics. These thermodynamic data provide useful information and references for not only UHV experimental studies but also practical applications at high temperature and pressure.

On the basis of the changes in Gibbs free energies of CO adsorption at very low pressure, the changes in CO coverage on iron surfaces at different temperatures can be obtained. This is, indeed, related to the thermal CO desorption, which can be detected with TPD spectroscopy under UHV conditions. As reported in our previous work,[42] the computed molecular desorption states (α_1-α_3) and the recombinative desorption state (β) on the Fe(100) surface under the consideration of CO dissociation at low coverage agree very well with the available experimental results. Now we compare our calculated CO desorption states at the range of p_{CO} = 10^{-9}−10^{-14} atmosphere on the other surfaces with the available experimental data in Table 7.

On the (110) surface, there are mainly two desorption states: one molecular CO adsorption (α) at 375−450 K and one recombinative desorption state (β) of the dissociated C and O atoms at 550−675 K. Actually, Gonzalez et al.[8] observed one low-temperature molecular desorption peak at ∼400−420 K and one recombinative desorption peak at about 675−800 K in the thermal desorption study of CO on the Fe(110) surface. Both theory and experiment agree very reasonably.

On the (111) surface, there are mainly two molecular desorption states at about 350−400 K (α_1) and 425−475 K (α_2) as well as one recombinative desorption state (β) at 525−575 K. Experimentally, Seip et al.[23] detected two low-temperature molecular CO desorption peaks at ∼340 K (α_1) and 420 K (α_2) with the exposure temperature at 220 K on the Fe(111) surface. Bartosch et al.[24] and Whitman et al.[25] also

dx.doi.org/10.1021/cs500287r | ACS Catal. 2014, 4, 1991−2005

Table 7. CO Desorption States and Temperatures on Six Iron Surfaces

surface	state	theory	experiment
(100)	α_1	275−300 K	220−250 K[12]
	α_2	325−375 K	306−340 K[12]
	α_3	400−450 K	400−440 K[12]
	β	700−750 K	750−820 K[12]
(110)	α	375−450 K	400−420 K[8]
	β	550−675 K	675−800 K[8]
(111)	α_1	350−400 K	325−340 K[24]
	α_2	425−475 K	400−420 K[24]
	β	525−575 K	650−750 K[24]
(210)	α	325−450 K	
	β	500−600 K	
(211)	α	300−400 K	
	β	450−575 K	
(310)	α	325−475 K	
	β	525−650 K	

found two molecular CO desorption peaks at about 325 K (α_1) and 400 K (α_2) with the exposure temperatures at 83 and 100 K. In addition, they also found a recombinative desorption state (β) of the dissociated C and O atoms at about 650−750 K. All these experimental results support our theoretically computed desorption states and temperatures.

However, it should be noted that our computed temperatures of the recombinative desorption states are generally lower than the reported experimental results, and this may result from the energy barrier of the recombination of surface C and O atoms to CO, which was not included in our thermodynamics method.

On the other high miller index surfaces, we also computed both the molecular (α) and dissociative desorption states (β) as well as the temperatures. On the Fe(210) surface, there are one molecular desorption state at about 325−450 K and one recombinative desorption state at about 500−600 K. On the Fe(211) surface, one molecular desorption state at about 300−400 K and one recombinative desorption state at about 450−575 K have been computed. On the Fe(310) surface, one

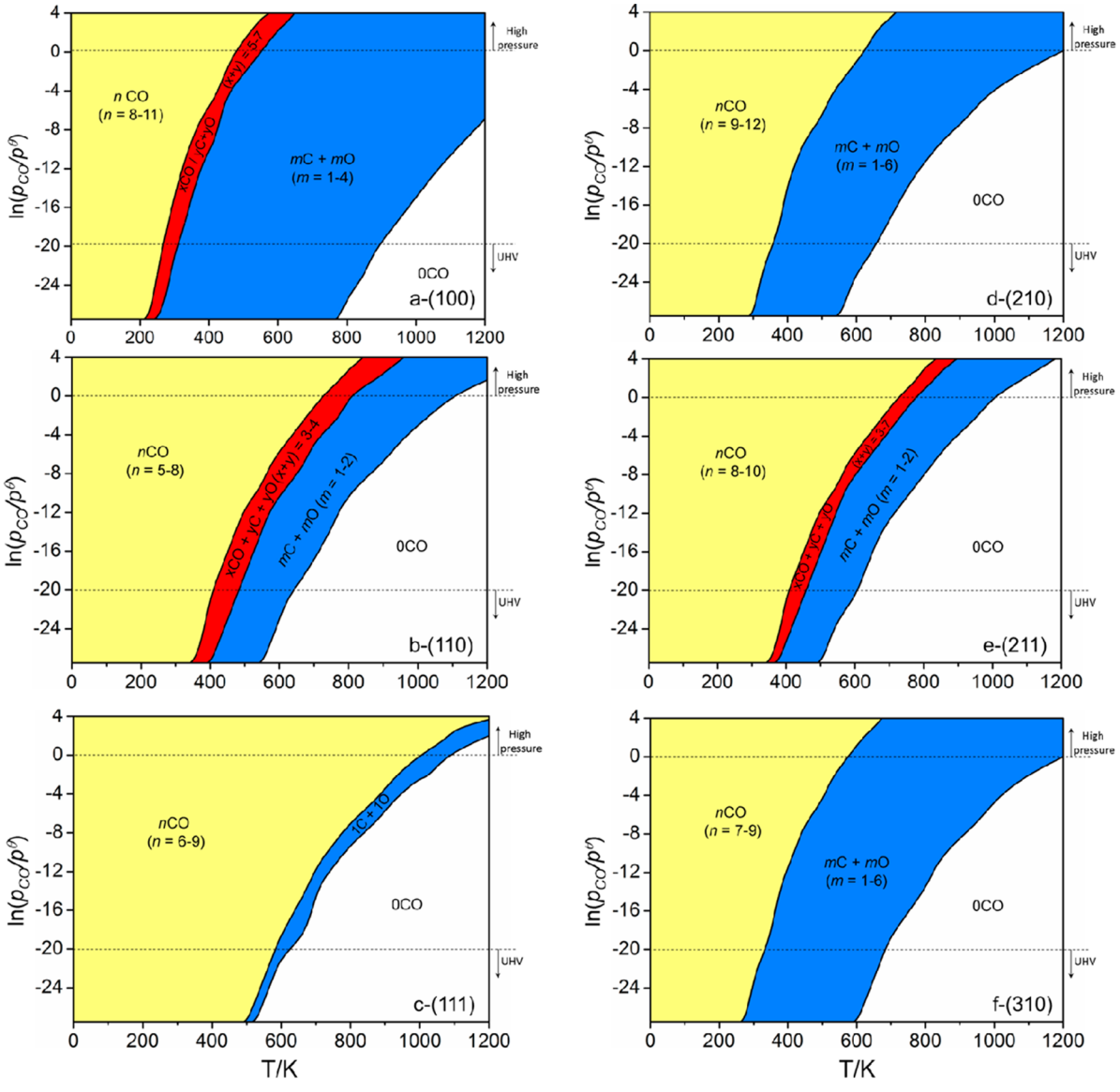

Figure 5. Phase diagram of stable CO adsorption states on six iron surfaces.

dx.doi.org/10.1021/cs500287r | ACS Catal. 2014, 4, 1991−2005

molecular desorption state at about 325−475 K and one recombinative desorption state at about 525−650 K from the adsorbed C and O atoms are found; however, there are no available UHV experimental studies of CO desorption on these surfaces. Therefore, our computed CO desorption states and temperatures on these high miller index surfaces might provide some references for further investigations using modern surface science techniques and analytical methods.

To consider the effects of temperature and pressure at the same time, we further plotted the phase diagrams (Figure 5) of stable CO adsorption states and coverage on the (100), (110), (111), (210), (211), and (310) surfaces. These phase diagrams provide useful thermodynamic information on CO adsorption states at high temperature and pressure, which is of great importance for industrial applications. Systematic comparisons show that each surface has characteristic regions at a given temperature and pressure, and this reveals their differences in CO adsorption states and coverage. On the basis of these phase diagrams, the six surfaces can be divided into two groups. The first group includes the (100), (110), and (211) surfaces that have a molecular adsorption region and a mixed molecular and dissociative adsorption region, as well as a fully dissociative region and clean surface region. The second group includes the (111), (210), and (310) surfaces, which have a molecular adsorption region, a fully dissociative region, and a clean surface region.

Actually, these thermodynamic phase diagrams provide new insights into the CO activation mechanism on iron surfaces that are quite different from previous studies at very low coverage, especially those high-temperature and -pressure regions. Taking T = 625 K and p_{CO} = 40 atm ($\ln(p_{CO}/p^{\theta})$ = 3.69) as reference, the adsorption states of CO on each surface present quite different thermodynamic characteristics; that is, only molecular CO adsorption is favorable on the (110), (111), and (211) surfaces; mixed molecular and dissociative CO adsorption are favorable on the Fe(100) surface; and only dissociative CO adsorption is favorable on the (210) and (310) surfaces.

3.6. Stretching Frequencies of Adsorbed CO Molecules. To provide some references for additional experimental studies, we have computed all CO stretching frequencies from the lowest to the saturated coverage on all surfaces. All the individual C−O vibrational data are listed in Supporting Information (Table S3−S8); and the range for each adsorption configuration at different coverage is listed in Table 8 for comparison.

On the Fe(100) surface, HREELS studies[18] found three molecular adsorption states having very different CO stretching frequencies: 1180−1245 cm^{-1} for the α_3 state and 1900−2070 cm^{-1} for the α_1 and α_2 states. At the lowest coverage, the computed CO stretching frequency is 1172 cm^{-1} at the 4-fold hollow, 1700 cm^{-1} at the bridge, and 1900 cm^{-1} at the top sites.[42] At the saturated coverage, the calculated CO stretching frequencies show mainly three ranges; 1179−1280 cm^{-1} for the 4-fold, 1800−1850 cm^{-1} for the bridge, and 2012 cm^{-1} for the top adsorption configurations.

On the Fe(110) surface, Erley[7] reported the shift of the C−O and Fe−C stretching frequencies from 1890 to 1950 cm^{-1} and from 456 to 500 cm^{-1} with exposure up to 0.7L (θ_{CO} = 1/4 ML), respectively, and from 1950 to 1985 cm^{-1} and 484 to 444 cm^{-1} with exposure in the range of 0.7−1.5 L (θ_{CO} = 1/2 ML). They attributed this to the presence of the designated and displaced off-center CO adsorptions on the top site with increasing coverage. Computationally, the C−O and Fe−C stretching frequencies are 1900 and 436 cm^{-1} at θ_{CO} = 1/12 ML (n_{CO} = 1), as well as 1888 and 1919 cm^{-1} and 436−440 cm^{-1} at θ_{CO} = 1/6 ML (n_{CO} = 2). At θ_{CO} = 1/4 ML (n_{CO} = 3, the same coverage as in experiment), the C−O and Fe−C stretching frequencies are 1889, 1894, and 1933 cm^{-1} and 438−447 cm^{-1}. These show reasonable agreement between theory and experiment in CO and Fe−C stretching frequencies with the exposure up to 0.7L (θ_{CO} = 1/4 ML).

Table 8. C−O Vibrational Frequencies (cm^{-1}) on Six Iron Surfaces

surface	state	theory	experiment
(100)	top	2012	1900−2070[18]
	bridge	1800−1850	
	4F	1179−1280	1180−1245[18]
(110)	top	1850−1956	1890−1985[7]
(111)	top	1907−1980	1945−2015[24]
	sh	1739−1856	1735−1860[24]
	dh	1482−1569	1325−1530[24]
(210)	top	1841−1918	
	4F	1115−1313	
(211)	top	1905−2011	
	bridge	1602−1881	
	4F	1192−1526	
(310)	top	1845−1920	
	4F	1104−1330	

At coverages higher than 1/4 ML, however, the computed stretching frequencies of the adsorbed CO molecules disagree with the experimental results. For n_{CO} = 4 (1/3 ML), for example, the most stable adsorption configurations are located on the long bridge sites with stretching frequencies in the range of 1688−1733 cm^{-1}. For n_{CO} = 5 and 6, the adsorbed CO molecules on the long bridge and 3-fold have stretching frequencies in the range of 1696−1789 cm^{-1}. For n_{CO} = 7 and 8, short bridge, long bridge, and 3-fold adsorption configurations are possible, and the CO stretching frequencies are 1723−1800 cm^{-1} for the long bridge and 3-fold adsorption configurations and 1820−1931 cm^{-1} for the short bridge adsorption configurations. It shows clearly that all of our computed CO stretching frequencies have much lower wave numbers than the reported range of 1950−1985 cm^{-1}.

Because CO stretching frequencies are directly associated with the C−O distances at the adsorbed equilibrium states, the shift of the CO frequencies to higher wave numbers upon an increase in the coverage should come from the weakening of the Fe−CO interaction and, therefore, the shortening of the CO distance. For one CO adsorption on Fe(110), for example, the computed CO stretching frequency is 1900 cm^{-1} at the top, 1733 cm^{-1} at the short bridge, 1659 cm^{-1} at the long bridge, and 1659 cm^{-1} at the 3-fold sites.

To understand this discrepancy at coverage higher than 1/4 ML, we computed the thermodynamically less stable adsorption configurations at the top site (Supporting Information, Figure S2). For n_{CO} = 4−6, the top adsorption configurations are less stable than their most stable adsorption configurations by 0.22, 0.25, and 0.30 eV, respectively. The computed CO stretching frequencies of these less stable top states are 1877−1947 cm^{-1} for n_{CO} = 4, 1875−1956 cm^{-1} for n_{CO} = 5, and 1847−1954 cm^{-1} for n_{CO} = 6. This agrees with the experimentally observed shift of the CO frequencies to higher wave numbers upon coverage increase. In particular, the CO frequencies for n_{CO} = 5 are in the range of the experimentally

dx.doi.org/10.1021/cs500287r | ACS Catal. 2014, 4, 1991−2005

detected 1890−1985 cm^{-1}.[7] In addition, the shift in the Fe−C frequencies from 442 to 401 cm^{-1} shows the same trend as also observed experimentally. It is also noted that for n_{CO} = 7−8, it is not possible to find such less-stable top adsorption configurations, as found for n_{CO} = 4−6. Similar discrepancies were also found by Stibor et al.[33] and Jiang et al.[34] They attributed the site preferences at different coverages to the choice of DFT methods.

On the basis of the computed CO stretching frequencies and energy differences, it is reasonable to conclude that the observed shift of the CO stretching frequencies might come from the shift of the equilibrium from the most stable adsorption configurations to the less stable top adsorption states at elevated temperature.

Early TPD studies of CO adsorption on the Fe(111) surface found three low-temperature molecular desorption states (α_0, α_1, and α_2). As discussed, we also found three CO molecular adsorption configurations coexisting on the Fe(111) surface, and they may correspond to the experimentally detected low-temperature desorption states. At the lowest coverage, the computed CO stretching frequency is 1906 cm^{-1} at the top, 1793 cm^{-1} at the shallow hollow, 1547 cm^{-1} at the deep hollow, and 1453 cm^{-1} at the 4-fold sites. At saturated coverage, the computed CO stretching frequencies are in the range of 1907−1980 cm^{-1} for the top; 1739−1856 cm^{-1} for shallow hollow; and 1482−1569 cm^{-1} for the 4-fold hollow adsorption configurations. Experimentally,[23−25] the three nondissociative CO adsorption configurations have C−O stretching frequencies of 1945−2015 (top), 1735−1860 (shallow hollow), and 1325−1530 cm^{-1} (deep hollow), respectively. However, we could not find the reported 1325 cm^{-1} frequency from the lowest to the saturated coverage.

On the Fe(210) surface (Supporting Information Figure S4) at the lowest coverage, the computed CO stretching frequencies are 1793 and 1865 cm^{-1} at the two top sites; 1739, 1644, and 1641 cm^{-1} at the three 3-fold sites; and 1115 cm^{-1} at the 4-fold hollow site. At the saturated coverage (n_{CO} = 12), top and 4-fold hollow adsorption configurations coexist, and the computed C−O stretching frequencies are in the range of 1841−1918 cm^{-1} for the top and 1115−1313 cm^{-1} for the 4-fold hollow adsorption configurations.

On the Fe(211) surface (Supporting Information Figure S5) at the lowest coverage, the computed CO stretching frequencies are 1701 and 1870 cm^{-1} at the two top sites, 1807 cm^{-1} at the bridge site, and 1274 cm^{-1} at the 4-fold hollow site. At saturated coverage (n_{CO} = 10), the coexistence of top, bridge, and 4-fold adsorption configurations becomes possible, and the C−O computed stretching frequencies are in the ranges of 1905−2011 cm^{-1} for the top, 1602−1881 cm^{-1} for the bridge, and 1192−1526 cm^{-1} for the 4-fold adsorption configurations.

On the Fe(310) surface (Supporting Information Figure S6) at lowest coverage, the computed CO stretching frequencies are 1772 and 1834 cm^{-1} at the two top sites, 1625 cm^{-1} at the 3-fold hollow site, and 1104 cm^{-1} at the 4-fold hollow site. At saturated coverage (n_{CO} = 9), both bridge and 4-fold hollow adsorption configurations are possible, and the C−O stretching frequencies are in the ranges of 1845−1920 cm^{-1} for the top and 1104−1330 cm^{-1} for the 4-fold adsorption configurations. However, there are no available experimental CO stretching frequencies on these three high-index surfaces for direct comparison with our calculated data.

CONCLUSION

Spin-polarized density functional theory computations have been carried out to study the adsorption, dissociation, and desorption of CO on the iron (100), (110), (111), (210), (211), and (310) surfaces at different coverages. The most stable adsorption configurations and the stepwise dissociation of the adsorbed CO molecules at different coverage have been computed. These detailed studies into the CO activation mechanisms provide some references about the initial stages of iron-based Fischer−Tropsch synthesis, in which CO adsorption and dissociation as well as surface carburization play the essential roles in the structures, stability, and activity of the catalysts. The computed CO desorption energies and dissociation barriers at different coverages and temperatures can be used for kinetic modeling, which is of practical importance.

At the lowest coverage (one CO adsorption), there are no direct correlations of the surface stabilities (surface energies) to the adsorption strengths (adsorption energies and CO stretching frequencies) as well as to the dissociation barriers and dissociation energies. This is because of their different adsorption sites and configurations. The most stable adsorption configurations and sites are coverage-dependent, and the coexistence of diverse adsorption configurations at different sites is possible at high coverage.

On the basis of the computed stepwise CO adsorption energies and dissociation barriers, equilibriums between molecular and dissociative adsorptions at high coverage have been found. On the Fe(100) surface, only dissociative adsorption is possible for n_{CO} = 1 and 2, whereas possible equilibrium between molecular and dissociative CO adsorptions are found for n_{CO} = 3−7. For n_{CO} = 8−11, only molecular CO adsorption can be found. On the Fe(110) surface, only dissociative CO adsorption is found for n_{CO} = 1, whereas equilibrium between CO + C + O and 2C + 2O is possible for n_{CO} = 2. For n_{CO} = 3 and 4, the surface adsorption states have mixed molecular and dissociative CO adsorptions coexisting; however, only molecular CO adsorption is found for n_{CO} = 5−8. On the Fe(111) surface, only dissociative CO adsorption is found for n_{CO} = 1; possible equilibrium between molecular (nCO) and dissociative (nC + nO) adsorptions is found for n_{CO} = 2, 3, and 5. For n_{CO} = 4, mixed molecular and dissociative CO coadsorption is possible. In contrast, only molecular CO adsorption is found for n_{CO} = 6−9.

On the Fe(210), only dissociative CO adsorption is favorable for n_{CO} = 1−6, whereas only molecular CO adsorption is possible for n_{CO} = 9−12. For n_{CO} = 7 and 8, the molecularly and dissociatively adsorbed CO molecules can coexist, and they might form equilibrium. On the Fe(211) surface, only dissociative CO adsorption is favorable for n_{CO} = 1−2, and only molecular CO adsorption is possible for n_{CO} = 5−10. In addition, the molecularly and dissociatively adsorbed CO molecules can coexist (n_{CO} = 3), and they might form an equilibrium (n_{CO} = 4) on the surface. On the Fe(310) surface, only dissociative adsorption is possible for n_{CO} = 1 and 3, whereas molecular and dissociative CO adsorptions are possible for n_{CO} = 2, 4, 5, and 6. For n_{CO} = 7−9, only molecular CO adsorption is preferred.

Along with the computed most stable molecular CO adsorption configurations at different coverages on the (100), (110), and (111) surfaces, the respective C−O and Fe−C stretching frequencies are in excellent agreement with the

dx.doi.org/10.1021/cs500287r | ACS Catal. 2014, 4, 1991−2005

available experimental data from high-resolution electron energy loss spectroscopy studies. Particularly, our computations clearly reveal that the experimentally observed shifts of the C−O and Fe−C stretching frequencies on the (110) surface up to the change of coverage come from the change in the equilibrium from the most stable adsorption configurations to the less stable top adsorption states at elevated temperature. The computed desorption states and temperatures on the (100), (110), and (111) surfaces are in perfect agreement with the available experimental data from temperature-programmed surface reaction studies. The computed CO adsorption and dissociation as well as desorption properties on the (210), (211), and (310) surfaces at different coverages invite modern experimental investigations. Our studies will provide useful references for the studies of CO related reaction mechanisms.

The interplay in CO activation mechanisms between theory and experiment on these iron surfaces reveals the intrinsic relationship of surface structures and catalyst activities in general and might contribute to a more rational catalyst development in the future.

■ ASSOCIATED CONTENT

Supporting Information

Details of the ab initio thermodynamics method; effects of zero-point energies (Table S1); available reported surface energies of iron surfaces (Table S2); vibrational frequencies of adsorbed CO at different coverages on six surfaces (Tables S3−S8); structures of those less stable one-CO adsorption configurations on five iron surfaces (Figure S1); structures and stepwise adsorption energies of CO on the five iron surfaces at different coverages (Figures S2−S6); structures for the dissociation of *n*CO on the five iron surfaces (Figures S7−S11); the most favored potential energy surface for CO dissociation at all coverage on five iron surfaces (Figures S12−16). This material is available free of charge via the Internet at http://pubs.acs.org.

■ AUTHOR INFORMATION

Corresponding Author

*E-mail: haijun.jiao@catalysis.de.

Notes

The authors declare no competing financial interest.

■ ACKNOWLEDGMENTS

This work was supported by the National Basic Research Program of China (No. 2011CB201406), the National Natural Science Foundation of China (No. 21073218), the Chinese Academy of Sciences, and Synfuels CHINA Co., Ltd. We also acknowledge general financial support from the BMBF and the state of Mecklenburg-Vorpommern.

■ REFERENCES

(1) Anderson, R. B. *The Fischer-Troposch Synthesis*; Academic Press: Orlando, FL, 1984; p 3.
(2) Kelly, R. D.; Goodman, D. W. In *The Chemical Physics of Solid Surfaces and Heterogeneous Catalysis*; King, D. A., Woodruff, D. P., Eds.; Vol. 4, Elsevier: Amsterdam, 1982; p 427.
(3) Fischer, F.; Tropsch, H. *Brennstoff Chem.* **1926**, *7*, 97−116.
(4) Brady, R. C., III; Pettit, R. *J. Am. Chem. Soc.* **1980**, *102*, 6181−6184.
(5) Yoshida, K.; Somorjai, G. A. *Surf. Sci.* **1978**, *75*, 46−60.
(6) Broden, G.; Gafner, G.; Bonzel, H. P. *Appl. Phys.* **1977**, *13*, 333−342.
(7) Erley, W. *J. Vac. Sci. Technol.* **1981**, *18*, 472−475.
(8) Gonzalez, L.; Miranda, R.; Ferrer, S. *Surf. Sci.* **1982**, *119*, 61−70.
(9) Wedler, G.; Ruhmann, H. *Surf. Sci.* **1982**, *121*, 464−486.
(10) Wedler, G.; Ruhmann, H. *Appl. Surf. Sci.* **1983**, *14*, 137−148.
(11) Benziger, J.; Madix, R. J. *Surf. Sci.* **1980**, *94*, 119−153.
(12) Moon, D. W.; Dwyer, D. J.; Bernasek, S. L. *Surf. Sci.* **1985**, *163*, 215−229.
(13) Cameron, S.; Dwyer, D. J. *Langmuir* **1988**, *4*, 282−288.
(14) Saiki, R. S.; Herman, G. S.; Yamada, M.; Osterwalder, J.; Fadley, C. S. *Phys. Rev. Lett.* **1989**, *63*, 283−286.
(15) Moon, D. W.; Cameron, S.; Zaera, F.; Eberhardt, W.; Carr, R.; Bernasek, S. L.; Gland, J. L.; Dwyer, D. J. *Surf. Sci. Lett.* **1987**, *180*, L123−L128.
(16) Moon, D. W.; Bernasek, S. L.; Lu, J. P.; Gland, J. L.; Dwyer, D. J. *Surf. Sci.* **1987**, *184*, 90−108.
(17) Dwyer, D. J.; Rausenberger, B.; Cameron, S. D.; Lu, J. P.; Bernasek, S. L.; Fischer, D. A.; Parker, D. H.; Gland, J. L. *Surf. Sci.* **1989**, *224*, 375−385.
(18) Moon, D. W.; Bernasek, S. L.; Dwyer, D. J.; Gland, J. L. *J. Am. Chem. Soc.* **1985**, *107*, 4363−4364.
(19) Benndorf, C.; Krüger, B.; Thieme, F. *Surf. Sci. Lett.* **1985**, *163*, L675−L680.
(20) Lu, J. P.; Albert, M. R.; Bernasek, S. L. *Surf. Sci.* **1989**, *217*, 55−64.
(21) Gladh, J.; Öberg, H.; Li, J. B.; Ljungberg, M. P.; Matsuda, A.; Ogasawara, H.; Nilsson, A.; Pettersson, L. G. M.; Öström, H. *J. Chem. Phys.* **2012**, *136*, 034702−9.
(22) Rochana, P.; Wilcox, J. *Surf. Sci.* **2011**, *605*, 681−688.
(23) Seip, U.; Tsai, M. C.; Christmann, K.; Kuppers, J.; Ertl, G. *Surf. Sci.* **1984**, *139*, 29−42.
(24) Bartosch, C. E.; Whitman, L. J.; Ho, W. *J. Chem. Phys.* **1986**, *85*, 1052−1060.
(25) Whitman, L. J.; Richter, L. J.; Gurney, B. A.; Villarrubia, J. S.; Ho, W. *J. Chem. Phys.* **1989**, *90*, 2050−2062.
(26) Mehandru, S. P.; Anderson, A. B. *Surf. Sci.* **1988**, *201*, 345−360.
(27) Blyholder, G.; Lawless, M. *Surf. Sci.* **1993**, *290*, 155−162.
(28) Meehan, T. E.; Head, J. D. *Surf. Sci.* **1991**, *243*, L55−L62.
(29) Nayak, S. K.; Nooijen, M.; Bernasek, S. L.; Blaha, P. *J. Phys. Chem. B* **2001**, *105*, 164−172.
(30) Sorescu, D. C.; Thompson, D. L.; Hurley, M. M.; Chabalowski, C. F. *Phys. Rev. B* **2002**, *66*, 035416.
(31) Bromfield, T. C.; Ferre, D. C.; Niemantsverdriet, J. W. *ChemPhysChem* **2005**, *6*, 254−260.
(32) Elahifard, M. R.; Jigato, M. P.; Niemantsverdriet, J. W. *ChemPhysChem* **2012**, *13*, 89−91.
(33) Stibor, A.; Kresse, G.; Eichler, A.; Hafner, J. *Surf. Sci.* **2002**, *507−510*, 99−102.
(34) Jiang, D. E.; Carter, E. A. *Surf. Sci.* **2004**, *570*, 167−177.
(35) Sun, X.; Forster, S.; Li, Q. X.; Kurahashi, M.; Suzuki, T.; Zhang, J. W.; Yamauchi, Y.; Baum, G.; Steidl, H. *Phys. Rev. B* **2007**, *75*, 035419.
(36) Chen, Y. H.; Cao, D. B.; Jun, Y.; Li, Y. W.; Wang, J.; Jiao, H. J. *Chem. Phys. Lett.* **2004**, *400*, 35−41.
(37) Huo, C. F.; Ren, J.; Li, Y. W.; Wang, J.; Jiao, H. J. *J. Catal.* **2007**, *249*, 174−184.
(38) Li, H. J.; Chang, C. C.; Ho, J. J. *J. Phys. Chem. C* **2011**, *115*, 11045−11055.
(39) Borthwick, D.; Fiorin, V.; Jenkins, S. J.; King, D. A. *Surf. Sci.* **2008**, *602*, 2325−2332.
(40) Lo, J. M.; Ziegler, T. *J. Phys. Chem. C* **2008**, *12*, 3692−3700.
(41) Sorescu, D. C. *J. Phys. Chem. C* **2008**, *112*, 10472−10489.
(42) Wang, T.; Tian, X.; Li, Y. W.; Wang, J.; Beller, M.; Jiao, H. *J. Phys. Chem. C* **2014**, *118*, 1095−1101.
(43) Mims, C. A.; McCandlish, L. E. *J. Phys. Chem.* **1987**, *91*, 929−937.
(44) Ojedaa, M.; Nabarb, R.; Nilekarb, A. U.; Ishikawaa, A.; Mavrikakisb, M.; Iglesia, E. *J. Catal.* **2010**, *272*, 287−297.
(45) Loveless, B. T.; Buda, C.; Neurock, M.; Iglesia, E. *J. Am. Chem. Soc.* **2013**, *135*, 6107−6121.

(46) Kresse, G.; Furthmüller, J. *Comput. Mater. Sci.* **1996**, *6*, 15−50.
(47) Kresse, G.; Furthmüller, J. *Phys. Rev. B* **1996**, *54*, 11169−11186.
(48) Blochl, P. E. *Phys. Rev. B* **1994**, *50*, 17953−17979.
(49) Kresse, G. *Phys. Rev. B* **1999**, *59*, 1758−1775.
(50) Perdew, J. P.; Burke, K.; Ernzerhof, M. *Phys. Rev. Lett.* **1996**, *77*, 3865−3868.
(51) Kresse, G.; Hafner, J. *Surf. Sci.* **2000**, *459*, 287−302.
(52) Methfessel, M.; Paxton, A. T. *Phys. Rev. B* **1989**, *40*, 3616−3621.
(53) Digne, M.; Sautet, P.; Raybaud, P.; Euzen, P.; Toulhoat, H. *J. Catal.* **2004**, *226*, 54−68.
(54) Henkelman, G.; Jónsson, H. *J. Chem. Phys.* **2000**, *113*, 9978−9985.
(55) Jiang, D. E.; Carter, E. A. *Phys. Rev. B* **2003**, *67*, 214103−214113.
(56) Sorescu, D. C. *Phys. Rev. B* **2006**, *73*, 155420−155436.
(57) Kittel, C. *Introduction to Solid State Physics*; Wiley: New York, 1996.
(58) Vitos, L.; Ruban, A. V.; Skriver, H. L.; Kollar, J. *Surf. Sci.* **1998**, *411*, 186−202.
(59) Spencer, M. J. S.; Hung, A.; Snook, I. K.; Yarovsky, I. *Surf. Sci.* **2002**, *513*, 389−398.
(60) Blonski, P.; Kiejna, A. *Vacuum* **2004**, *74*, 179−183.
(61) Blonski, P.; Kiejna, A. *Surf. Sci.* **2007**, *601*, 123−133.
(62) Huo, C. F.; Wu, B. S.; Gao, P.; Yang, Y.; Li, Y. W.; Jiao, H. *Angew. Chem. Int. Ed.* **2011**, *50*, 7403−7406.
(63) Wang, T.; Wang, S. G.; Luo, Q. Q.; Li, Y. W.; Wang, J.; Beller, M.; Jiao, H. *J. Phys. Chem. C* **2014**, *118*, 4181−4188.
(64) Reuter, K.; Scheffler, M. *Phys. Rev. B* **2001**, *65*, 035406.
(65) Reuter, K.; Scheffler, M. *Phys. Rev. B* **2003**, *68*, 045407.
(66) Li, W.-X.; Stampfl, C.; Scheffler, M. *Phys. Rev. .B* **2003**, *68*, 165412.
(67) Rogal, J.; Reuter, K.; Scheffler, M. *Phys. Rev. .B* **2004**, *69*, 075421.
(68) Grillo, M. E.; Ranke, W.; Finnis, M. W. *Phys. Rev. .B* **2008**, *77*, 075407.
(69) Aray, Y.; Vidal, A. B.; Rodriguez, J.; Grillo, M. E.; Vega, D.; Coll, D. S. *J. Phys. Chem. C* **2009**, *113*, 19545−19557.
(70) Zasada, F.; Piskorz, W.; Cristol, S.; Paul, J. F.; Kotarba, A.; Sojka, Z. *J. Phys. Chem. C* **2010**, *114*, 22245−22253.
(71) Wang, T.; Liu, X. W.; Wang, S. G.; Huo, C. F.; Li, Y. W.; Wang, J.; Jiao, H. *J. Phys. Chem. C* **2011**, *115*, 22360−22368.
(72) Wang, T.; Wang, S. G.; Li, Y. W.; Wang, J.; Jiao, H. J. *J. Phys. Chem. C* **2012**, *116*, 6340−6348.
(73) Wang, T.; Li, Y. W.; Wang, J.; Beller, M.; Jiao, H. *J. Phys. Chem. C* **2014**, *118*, 3162−3171.
(74) Luo, Q.; Beller, M.; Jiao, H. *J. Theor. Comput. Chem.* **2013**, *12*, 1330001−28.
(75) Cao, D.-B.; Li, Y.-W.; Wang, J.; Jiao, H. *J. Phys. Chem. C* **2008**, *112*, 14884−14890.
(76) Munter, T. R.; Bligaard, T.; Christensen, C. H.; Nørskov, J. K. *Phys. Chem. Chem. Phys.* **2008**, *10*, 5202−5206.
(77) Liu, Z. P.; Hu, P. *J. Chem. Phys.* **2001**, *123*, 8244−8247.
(78) Liu, Z. P.; Hu, P. *J. Am. Chem. Soc.* **2001**, *123*, 12596−12604.
(79) Michaelides, A.; Liu, Z. P.; Zhang, C. J.; Alavi, A.; King, D. A.; Hu, P. *J. Am. Chem. Soc.* **2003**, *125*, 3704−3705.